Nonsimilar Nature of the Laminar Boundary Layer

WILLIAM F. GALLO,* JOSEPH G. MARVIN,* AND A. VERNON GNOS†
NASA Ames Research Center, Moffett Field, Calif.

The effect of including the streamwise history or nonsimilar terms in the usual transformed laminar boundary-layer equations is studied at three locations on a typical, blunted, compression surface. The locations represent regions of mildly favorable, mildly adverse, and strongly adverse pressure gradient. Theoretical boundary-layer solutions were obtained at the three stations by numerically solving the laminar boundary-layer equations both with and without the streamwise history terms included. Both solutions are compared with experimental boundary-layer data. The results indicate that in the presence of a strong adverse pressure gradient the solutions exhibit a significant difference when the streamwise history terms are considered. The largest differences appear in velocity profile and displacement thickness with the data confirming the validity of the fully nonsimilar solution.

Nomenclature

f = dimensionless stream function
f_η = dimensionless velocity in streamwise direction, u/u_e
g = dimensionless total enthalpy, H/H_0
H = total enthalpy, $h + (u^2/2)$
h = static enthalpy
M = Mach number
n = index, = 1 for axisymmetric, = 0 for two-dimensional flow
p = pressure
r = cylindrical radius of body
T = temperature
u = velocity in local streamwise direction
x = coordinate in local streamwise direction
y = coordinate normal to local streamwise direction
β = pressure gradient parameter [Eq. (3a)]
γ = ratio of specific heats
δ^* = displacement thickness, $\int_0^\infty \left(1 - \frac{\rho u}{\rho_e u_e}\right) dy$
η = transformed normal coordinate [Eq. (1)]
Θ = momentum thickness, $\int_0^\infty \frac{\rho u}{\rho_e u_e}\left(1 - \frac{u}{u_e}\right) dy$
μ = viscosity
ξ = transformed coordinate in streamwise direction [Eq. (2)]
ρ = density
σ = Prandtl number
ϕ = dimensionless density-viscosity product, $\rho\mu/\rho_e\mu_e$

Subscripts

e = boundary-layer edge
0 = stagnation point
w = wall
η = partial differentiation with respect to η
ξ = partial differentiation with respect to ξ
∞ = freestream value

Introduction

BOUNDARY-layer development in the presence of adverse pressure gradients has received renewed attention in the study of compression surfaces on hypersonic inlets. As distinguished from supersonic inlets where much of the boundary layer is bled off, the higher temperatures of the boundary layer in a hypersonic inlet will preclude bleeding. It is also expected that the boundary-layer thickness will be large due to the long length of run found on most proposed inlet configurations. This, coupled with the small throat heights resulting from the large contraction ratios, will often result in a large percentage of the throat flow being made up of boundary layer. Because the boundary layer becomes such an important consideration in inlet design, much new effort is being focused on the behavior of boundary layers in hypersonic flows with adverse pressure gradients.

In regions of favorable pressure gradients, reasonably good predictions of boundary-layer behavior have been obtained from solutions of the laminar boundary-layer equations utilizing the assumption of local similarity. This technique[1-3] reduces the basic boundary-layer equations from partial differential equations to a system of ordinary differential equations by ignoring the streamwise history of the flow except for the history implied in the definition of the transformed coordinates. One attempted improvement on this analysis was first shown by Thwaites.[4] By using correlations between wall shear stress, pressure gradient, and the ratio of displacement to momentum thickness, he devised an integral method applicable to incompressible flow with pressure gradients. Extensions to adiabatic wall with unity Prandtl number[5] and compressible flow with heat transfer[6] and real gas[7] have been made. None of the methods have demonstrated applicability in regions of adverse pressure gradient, however, and all of them appear to have basic deficiencies. Further discussion of local similarity assumptions may be found in Hayes and Probstein[8] and others.[9,10]

Recently reported methods[11,12] now make possible the practical solution of the complete boundary-layer equations including the streamwise history. Moreover, recent availability of large high Mach number test facilities also make it possible to obtain more reliable data. Marvin and Sinclair[13] took advantage of these two developments to investigate the consequences of the local similarity assumption in regions of large favorable pressure gradient. They solved the laminar boundary-layer equations, transformed to the Lees-Dorodnitsyn coordinates both with and without the assumption of local similarity. Their study provided a particularly good comparison since the equations compared were exactly the same except for the streamwise derivatives and were solved using the same computer program. This eliminated many uncertainties usually found in such studies. Marvin's study concluded that for a large favorable pressure gradient, as produced by the flow over the corner of a flat-nosed blunt body, the locally similar solutions gave satisfactory predictions of heat transfer and that little difference existed between the boundary-layer profiles predicted by the two solutions.

The purpose of the present study is to investigate the applicability of the assumption of local similarity in a region

Presented as Paper 69-35 at the AIAA 7th Aerospace Sciences Meeting, New York, January 20–22, 1969; submitted February 5, 1969; revision received June 16, 1969.

* Research Scientist. Associate Fellow AIAA.
† Research Scientist. Member AIAA.

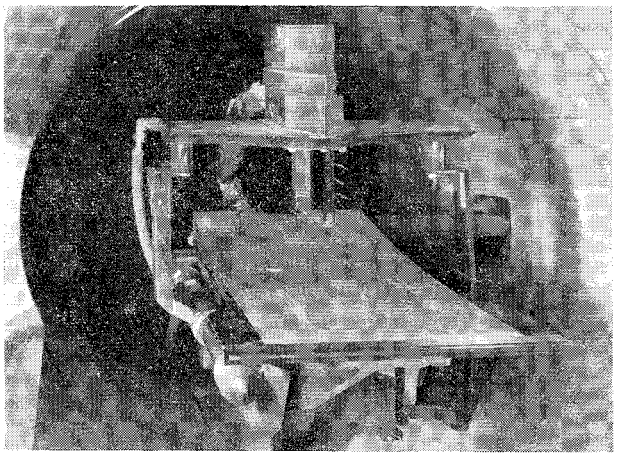

Fig. 1 Photograph of compression surface model.

of unfavorable pressure gradient. This is done by comparing predictions of boundary-layer profiles and momentum and displacement thicknesses using the similar and nonsimilar boundary-layer solutions with experimental results obtained on a large-scale compression surface model. Individual terms of the equations are also evaluated to aid in understanding the results and are discussed in the Appendix.

Laminar Boundary-Layer Equations

Nonsimilar Equations

The Lees-Dorodnitsyn transformations[14] are utilized to transform the x and y coordinates of the usual boundary-layer equations to η and ξ. By definition,

$$\eta = \frac{\rho_e u_e r^n}{(2\xi)^{1/2}} \int_0^y \frac{\rho}{\rho_e}\, dy \tag{1}$$

$$\xi = \int_0^x \rho_e \mu_e u_e r^{2n} dx \tag{2}$$

The following equations result:
Momentum:

$$(\phi f_{\eta\eta})_\eta + f f_{\eta\eta} + \beta\left[\frac{\rho_e}{\rho} - f_\eta^2\right] = 2\xi(f_\eta f_{\eta\xi} - f_\xi f_{\eta\eta}) \tag{3}$$

where

$$\beta = 2d\ \ln u_e / d\ \ln \xi \tag{3a}$$

Energy:

$$\left[\frac{\phi g_\eta}{\sigma}\right]_\eta + f g_\eta + \frac{u_e^2}{H_0}\left[\left(1 - \frac{1}{\sigma}\right)\phi f_\eta f_{\eta\eta}\right]_\eta = 2\xi(f_\eta g_\xi - f_\xi g_\eta) \tag{4}$$

To complete the system of equations, the transport and thermodynamic properties of air are expressed as functions of enthalpy in the manner described in Refs. 7 and 8. For example,

$$\frac{\rho\mu}{(\rho\mu)_{\text{ref}}} = F\left[\frac{h}{h_{\text{ref}}}\right] \tag{5}$$

The equations are solved by iterative techniques using the boundary conditions

$$\left.\begin{aligned} f_\eta(0,\xi) &= 0 \\ f_\eta(\infty,\xi) &= 1 \\ g(0,\xi) &= g_w(\xi) \\ g(\infty,\xi) &= 1 \end{aligned}\right\} \tag{6}$$

The equations are solved as ordinary differential equations in η by prescribing initial conditions for $f_{\eta\eta}$ and g_η at $\eta = 0$ and iteratively changing these conditions until the edge conditions are satisfied as $\eta \to \infty$. The outer boundary conditions were assumed to be satisfied when

$$f_{\eta\eta}(\eta \to \infty),\ g_\eta(\eta \to \infty) \leq 0.005$$

The ξ derivatives are obtained using implicit three-point difference equations. Further details of the method of solution are given in Refs. 7 and 8.

Locally Similar Equations

Approximate solutions to the full set of equations [Eqs. (3) and (4)] have been obtained by utilizing the assumption of so-called local similarity. This assumption neglects the derivatives with respect to ξ, thus reducing the partial differential equations to ordinary differential equations in η alone, facilitating solution. The result then is a series of local solutions independent of the boundary-layer history except as implied in the definition of the transformed coordinate, ξ, The equations neglecting the terms with derivatives in ξ are
Momentum:

$$(\phi f_{\eta\eta})_\eta + f f_{\eta\eta} + \beta\left[\frac{\rho_e}{\rho} - f_\eta^2\right] = 0 \tag{7}$$

Energy:

$$\left[\frac{\phi g}{\sigma}\right]_\eta + f g_\eta + \frac{u_e^2}{H_0}\left[\left(1 - \frac{1}{\sigma}\right)\phi f_\eta f_{\eta\eta}\right]_\eta = 0 \tag{8}$$

These equations were solved in the same manner as Eqs. (3) and (4) using the same boundary conditions of Eq. (6). The solution is somewhat simpler since the streamwise terms are neglected.

Experiment

Model and Test Facility

The model (Fig. 1), whose coordinates are listed in Table 1, is an isentropic compression surface, 48 in. in length, with a slightly blunted nose radius of 0.188 in. To prevent warping of the leading edge from the high stagnation temperatures, water cooling tubes in the leading edge were employed. Surface temperatures were measured by thermocouples mounted in the surface of the model at various longitudinal stations. It was found that due to the short running times and large model mass surface temperatures were nearly constant along the length of the model except for the immediate nose region. Surface pressures were measured by orifices located at various longitudinal stations. Spanwise surface pressure measurements were also made to confirm the two-dimensional character of the flow.

The model was tested in the Ames 3.5-ft hypersonic wind tunnel at a freestream Mach number of 10.5. The nominal freestream total temperature was 1900°R, the freestream

Table 1 Model coordinates

X, in.	Y, in.	X, in.	Y, in.
0	0	24	1.450
10	0.524	26	1.626
11	0.578	28	1.820
12	0.634	30	2.038
13	0.692	32	2.280
14	0.752	34	2.540
15	0.813	36	2.816
16	0.874	38	3.108
17	0.936	40	3.414
18	1.000	42	3.734
19	1.066	44	4.070
20	1.136	46	4.422
22	1.286	48	4.790

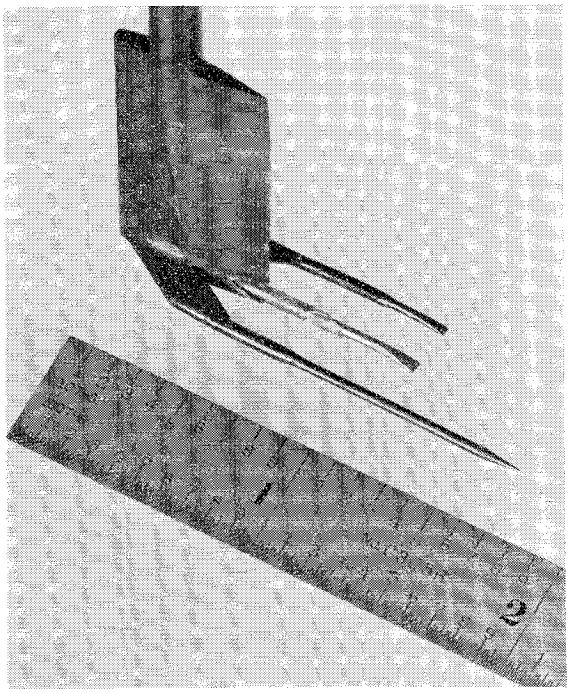

Fig. 2 Photograph of boundary-layer probe.

total pressure was 1800 psia, and the resulting Reynolds number was approximately 2 million per foot. Additional details concerning the facility are given in Ref. 15.

Profile Determination

Velocity profiles were determined, from measured Pitot and static pressure and total temperature, using a three-pronged movable probe (see Fig. 2) mounted on an overhead carriage. Profiles were obtained at three survey stations, 11.2, 26.2, and 39.1 in. downstream of the leading edge. The measured temperature was modified by a probe calibration factor experimentally obtained and similar to that described in Ref. 16. The edge of the boundary layer was determined experimentally from Pitot pressure, temperature, and velocity profiles. Comparisons with the velocity and Pitot profiles obtained from an inviscid method of characteristics also aided in determining the boundary-layer edge.

Results and Discussion

Theoretical boundary-layer velocity profiles were obtained using edge conditions obtained from measured surface static and impact pressures along with measured total test conditions. The boundary-layer calculations were begun at the stagnation point of the small blunt leading edge and for these

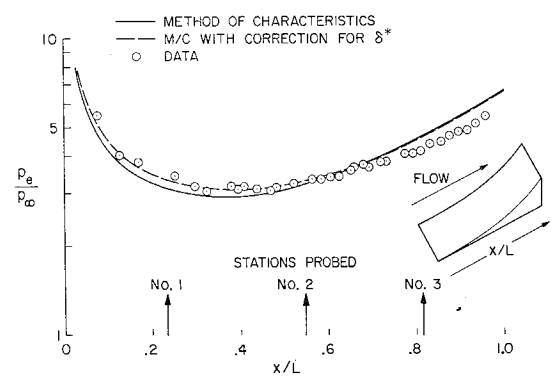

Fig. 3 Longitudinal distribution of pressure along compression surface.

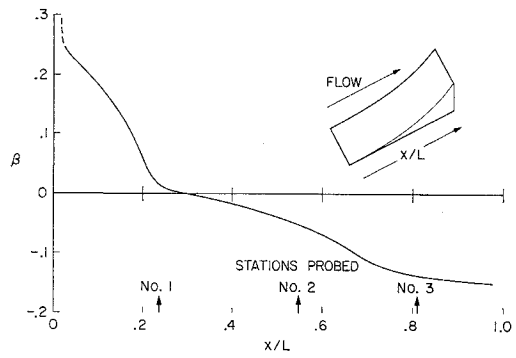

Fig. 4 Longitudinal distribution of pressure gradient parameter along compression surface.

edge conditions theoretical values were used. It should be pointed out that although the freestream Mach number is 10.5, the small nose bluntness and the compression surface reduces the Mach number at the boundary-layer edge to about 3.2 for the three stations considered. Figure 3 shows the longitudinal distribution of surface static pressure along with a theoretical distribution obtained from a method of characteristics solution using initial conditions obtained from a blunt-body solution.[17] A second theoretical distribution taking into account a displacement thickness obtained from the boundary-layer solution resulted in better agreement in pressure distribution, particularly at the first two stations probed. Agreement between theory and experiment is acceptable, certainly up to the last boundary-layer survey station at $X/L = 0.81$. Both inviscid theory and experiment also indicated that static pressures normal to the surface were practically constant for a distance at least equal to the predicted boundary-layer height.

Figure 4 shows the longitudinal variation of the pressure gradient parameter β computed from Eq. (3a). The initial positive β results from the small nose blunting; β remains positive up to about 15 in. along the surface where the surface turning produces compression and a negative β.

Velocity Profiles

Theoretical velocity profiles were obtained from solutions to both the similar and nonsimilar boundary-layer equations and are shown along with the experimental results in Figs. 5–7. The first boundary-layer survey station probed was 11.2 in. downstream of the nose in a region of slightly favorable pressure gradient ($\beta = 0.0235$) (Fig. 5). Little difference appears between the profiles predicted from either solution. The experimental data show reasonable agreement with theory, when it is considered that physical heights are compared. It may be noted that near the surface, probe interference effects strongly affect the data (e.g., data less than ~0.07 in.). The results are as expected and confirm the

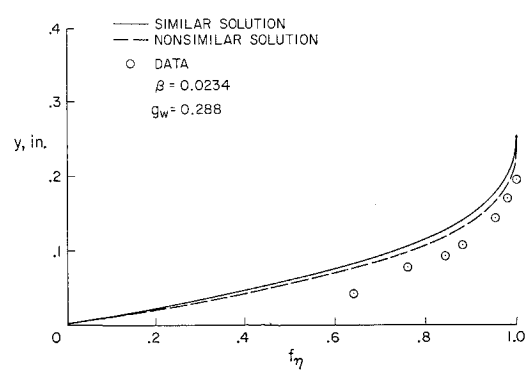

Fig. 5 Boundary-layer velocity profile at $X/L = 0.23$.

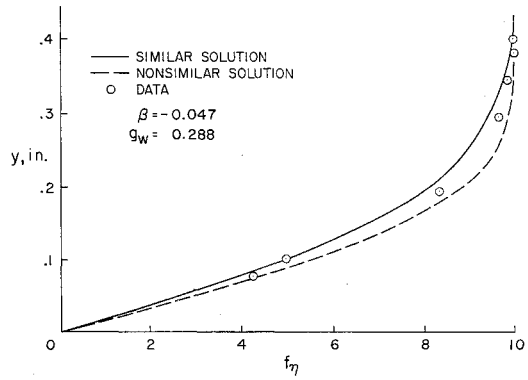

Fig. 6 Boundary-layer velocity profile at X/L = 0.55.

conclusions of others, namely, that for favorable pressure gradients (here mildly favorable gradients), the assumption of local similarity provides reasonable solutions.

The second station, 26.2 in. downstream of the nose, is in a region of slightly adverse pressure gradient ($\beta = -0.047$). The predicted and measured velocity profiles at this station are presented in Fig. 6. The data fall between the two predictions and either prediction appears reasonable.

At the third station, 39.1 in. from the nose, where the pressure gradient is strongly adverse ($\beta = -0.138$), there is

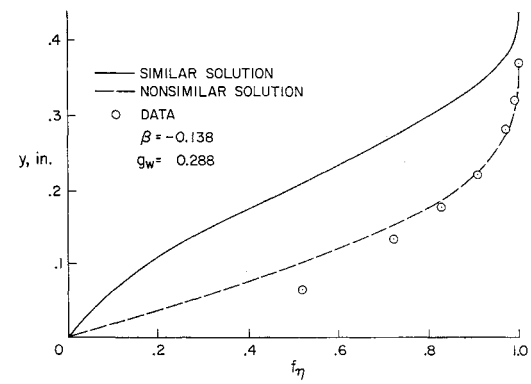

Fig. 7 Boundary-layer velocity profile at X/L = 0.81.

a marked difference between the velocity profiles predicted by the nonsimilar and the locally similar solutions as shown in Fig. 7. The experimental profile agrees with the predicted nonsimilar profile and confirms the validity of the solution that considers the streamwise history. Thus, on this compression surface in the region where the pressure gradient was strongly adverse, it is necessary to include the boundary-layer history to achieve a reasonable prediction of the velocity profile.

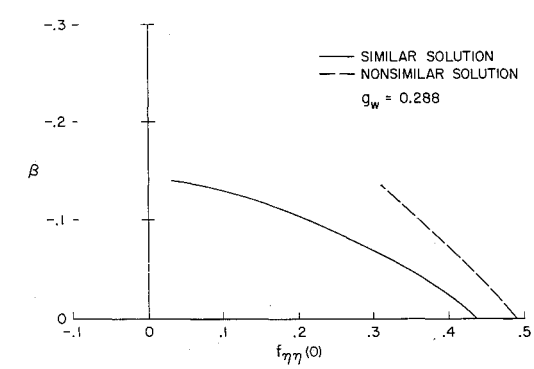

Fig. 8 Wall shear vs pressure gradient parameter along compression surface.

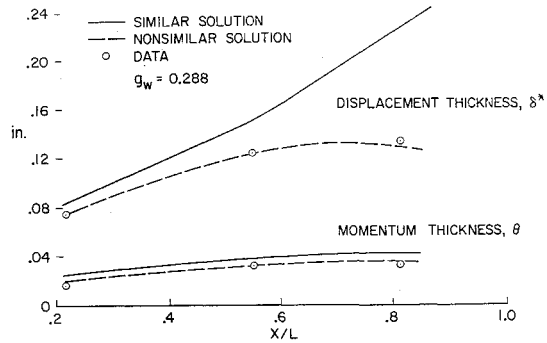

Fig. 9 Boundary-layer integral properties for compression surface.

Incipient Separation

The importance of retaining the nonsimilar terms in the boundary-layer prediction also manifests itself when boundary-layer separation is considered. Figure 7 indicates that the velocity profile as predicted by the similar solution is incipient to separation. This condition is also demonstrated in Fig. 8, which shows the wall shear, $f_{\eta\eta}(0)$, plotted versus the pressure gradient parameter, β, for various locations along the compression surface where β was negative. The similar solution predicts a significantly lower wall shear than does the nonsimilar solution for the same pressure gradient. The similar solution also indicates a rapid approach to zero wall shear or, to separation as indicated by the flat slope of the curve near the value of $\beta = -0.138$, the last survey station. The nonsimilar solution indicates a slower approach to separation, which is consistent with the data from the velocity profiles. As a matter of interest, it was determined that for the subject compression surface, nonsimilar solutions could be obtained for larger negative values of β before the shear approached zero. It may be concluded that retaining the nonsimilar terms in the boundary-layer equations in the present case leads to significantly different predictions of the separation point, the nonsimilar solution predicting separation further downstream than the similar.

Integral Properties

Predictions of the integral properties, such as boundary-layer momentum and displacement thicknesses, are also affected by retention of the nonsimilar terms in the boundary-layer equations. Figure 9 presents a comparison of predicted and experimental displacement and momentum thicknesses along the compression surface. The momentum thickness is slightly lower for the nonsimilar solution. The predicted displacement thicknesses, though, differ considerably in the adverse pressure gradient region and here only the results from the nonsimilar solution agree with the

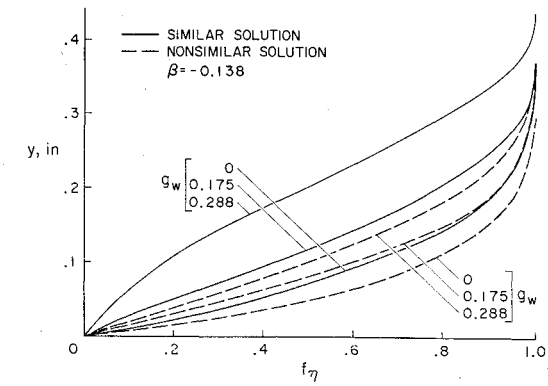

Fig. 10 Boundary-layer velocity profiles for different wall cooling ratios.

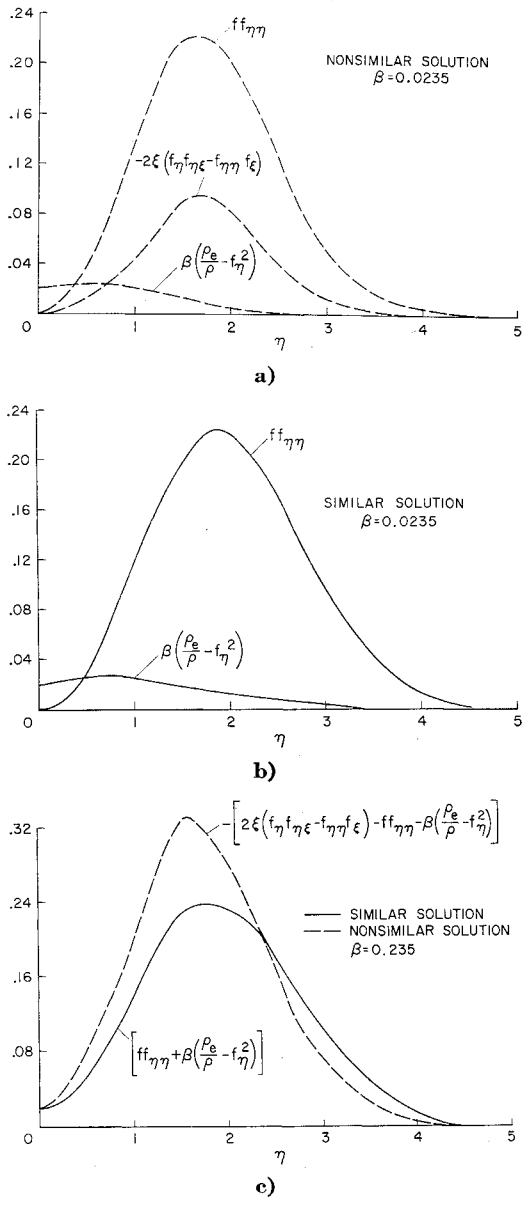

Fig. 11 Terms of the laminar boundary-layer momentum equation at $X/L = 0.23$; a) individual terms, nonsimilar; b) individual terms, similar; c) summation of terms, similar and nonsimilar.

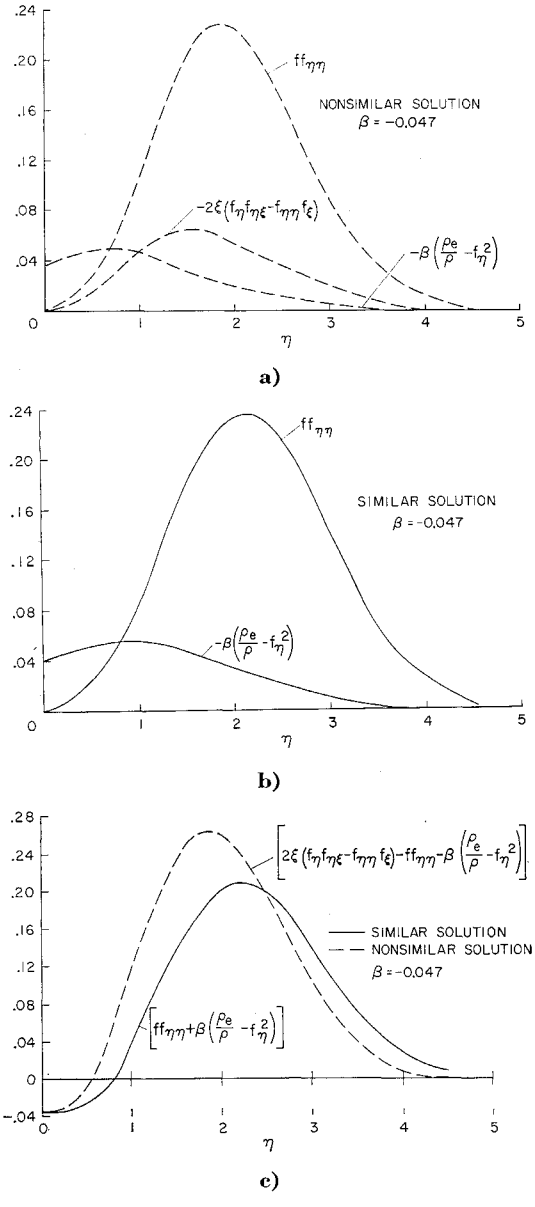

Fig. 12 Terms of the laminar boundary-layer momentum equation at $X/L = 0.55$; a) individual terms, nonsimilar; b) individual terms, similar; c) summation of terms, similar and nonsimilar.

measurements. The consequences of overestimating the displacement thickness may be strongly reflected, for example, in the design of a hypersonic inlet, wherein the displacement thickness is used to give an effective inviscid flow contour.

Effects of Wall Cooling

To determine whether the differences exhibited between the locally similar and nonsimilar solutions depended on wall temperature, solutions were performed for different wall cooling ratios. Figure 10 presents the resulting velocity profiles at the last survey station for the similar and nonsimilar solutions. There is a significant effect of wall cooling ratio on both solutions. Although the profiles are different for each of the wall cooling ratios investigated, the largest difference appears at $g_w = 0.288$, where the similar solution exhibits a profile incipient to separation as previously shown.

Conclusions

Comparisons of boundary-layer characteristics predicted using nonsimilar and locally similar forms of the boundary-layer equations have been made with data obtained on a compression surface model. The following conclusions were reached:

1) The full set of nonsimilar solutions, which accounts for streamwise boundary-layer history, gave predictions of velocity profiles and displacement and momentum thicknesses that compared well with data.

2) The locally similar solutions, which neglect streamwise boundary-layer history, failed to give accurate predictions in the region of strong adverse pressure gradient, although in the mildly favorable and mildly adverse pressure gradient region the predictions were reasonable.

Appendix

Influence of Nonsimilar Terms

A qualitative understanding of the differences in predicted velocity profiles in regions of adverse pressure gradient can be achieved by examining the behavior of the terms in the momentum equation as a function of η. For this purpose,

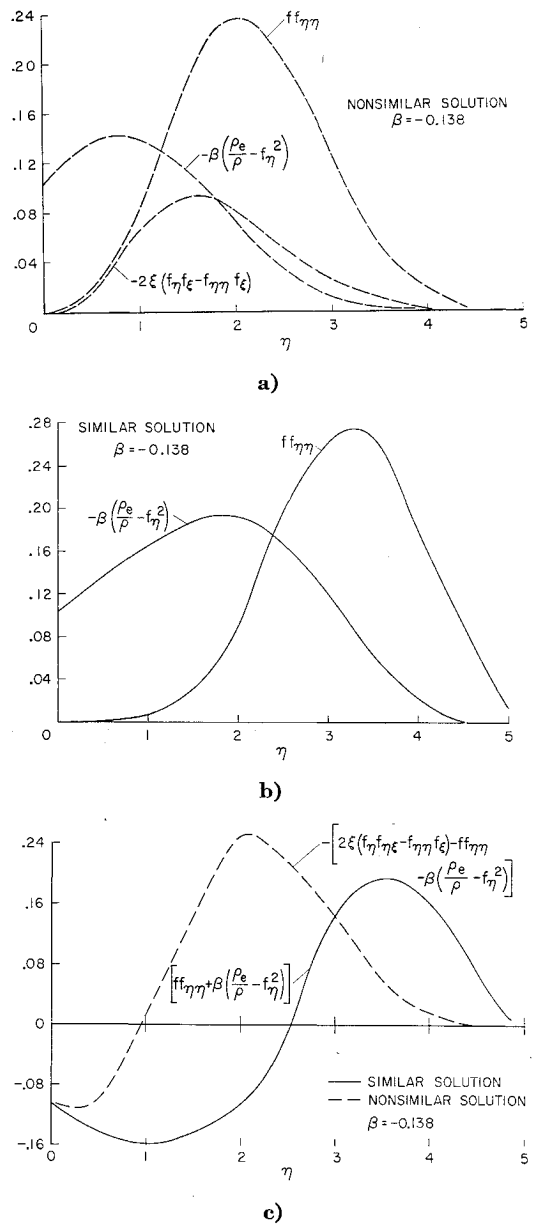

Fig. 13 Terms of the laminar boundary-layer momentum equation at $X/L = 0.81$; a) individual terms, nonsimilar; b) individual terms, similar; c) summation of terms, similar and nonsimilar.

it is convenient to rewrite Eq. (3) as

$$(\phi f_{\eta\eta})_\eta = 2\xi(f_\eta f_{\eta\xi} - f_\xi f_{\eta\eta}) - f f_{\eta\eta} - \beta\left[\frac{\rho_e}{\rho} - f_\eta^2\right] \quad \text{(A1)}$$

The corresponding locally similar equations are obtained by removing the nonsimilar term, $2\xi(f_\eta f_{\eta\xi} - f_\xi f_{\eta\eta})$.

The terms on the right-hand sides of Eq. (A1) at each survey station are plotted in Figs. 11, 12, and 13. Parts a and b of the figures show the terms obtained from the nonsimilar and locally similar solutions, respectively. Part c compares the summation of these terms for the two solutions. For positive values of β [see Fig. 11a], both the nonsimilar term, which is negative, and the pressure gradient term, $\beta(\rho_e/\rho f_\eta^2)$, which is preceded by a negative sign in the equation, influence the solution in the same way. That is, they increase the absolute value of the right-hand side of Eq. (A1), which results in an increase in velocity gradient at the wall for the nonsimilar solution over the similar solution. On the other hand, for negative values of β [Figs. 12a and 13a], the nonsimilar term and the pressure gradient term have opposite signs. The net result is a decrease in the absolute value of the right-hand side of Eq. (A1). The right-hand side of the equation, including the nonsimilar term, is still larger than when it is neglected as evidenced in Figs. 12c and 13c. Thus, whenever the nonsimilar terms are included, the velocity gradient at the wall or wall shear is always greater than that obtained by neglecting nonsimilar terms. This increase in velocity gradient will result in a fuller velocity profile (cf. results from Figs. 6 and 7).

Other investigators (e.g., Refs. 1 and 2) have suggested that the use of locally similar solutions may be justified when the magnitude of the nonsimilar terms is negligible as compared with the other terms. The present results indicate that at each of the three survey stations the nonsimilar term is not negligible (Figs. 11a, 12a, and 13a) yet the similar solutions yield reasonable predictions at the first and second station although not at the third station. Thus it is apparent that merely evaluating the magnitude of the nonsimilar term would not be sufficient to determine when locally similar solutions might be utilized. Further, it is suggested from the present results that only where β is a large negative quantity, or in other words, regions of strong adverse pressure gradients is it necessary to use the more complex nonsimilar solutions.

In Fig. 13b, $ff_{\eta\eta}$ does not achieve as small a value at large η for the locally similar solution as it does at the other two stations. The usual criteria for achieving a converged solution were that $f_{\eta\eta}(\eta \to \infty)$ and $g_\eta(\eta \to \infty) \leq 0.005$. At the last station where $\beta = -0.138$ it was not possible to satisfy this condition and convergence was determined to be satisfied when $f_{\eta\eta}(\eta \to \infty)$ and $g_\eta(\eta \to \infty)$ was ≤ 0.01. Refinements to the solution were attempted by increasing η to very large values and by computing a family of solutions for β close to the nominal value. No improvement in the value of $f_{\eta\eta}(\eta \to \infty)$ could be obtained. Although some error in the solution may be involved, the magnitude of the error is felt to be negligible.

Observation of Fig. 13c, which is the summation of the individual terms at the last station, shows that the locally similar solution is quite different from the nonsimilar solution.

It may be noted that the summation of similar terms is equal to $(f_{\eta\eta})_\eta$ according to Eq. (7). Integrating the curve over the range of η is then proportional to the wall shear $f_{\eta\eta}(0)$. Bearing in mind the signs involved, it may be noted that the net result of integrating the area would tend toward zero, indicating close to zero shear at the wall. This observation is confirmed by Fig. 8, which shows wall shear to be approaching zero at this station.

References

[1] Fay, J. A. and Riddell, R. D., "Theory of Stagnation Point Heat Transfer in Dissociated Air," *Journal of the Aeronautical Sciences*, Vol. 25, No. 2, Feb. 1958, pp. 73–85.

[2] Kemp, N. H., Rose, P. H., and Detra, R. W., "Laminar Heat Transfer Around Blunt Bodies in Dissociated Air," *Journal of the Aerospace Sciences*, Vol. 26, No. 7, July 1959, pp. 421–430.

[3] Cohen, C. B. and Reshotko, E., "Similar Solutions for the Compressible Laminar Boundary Layer with Heat Transfer and Pressure Gradient," Rept. 1293, 1956, NACA.

[4] Thwaites, B., "Approximate Calculation of the Laminar Boundary Layer," *Aero Quarterly*, Vol. I, Pt. III, Nov. 1949, pp. 245–280.

[5] Kote, N. and Crabtree, L. T., "Simplified Laminar Boundary Layer Calculations for Bodies of Revolution and for Yawed Wings," *Journal of the Aeronautical Sciences*, Vol. 19, No. 8, Aug. 1952, pp. 553–565.

[6] Cohen, C. B. and Reshotko, E., "The Compressible Laminar Boundary Layer with Heat Transfer and Arbitrary Pressure Gradient," Rept. 1294, 1956, NACA.

[7] Beckwith, I. E. and Cohen, N. B., "Application of Similar Solutions to Calculation of Laminar Heat Transfer on Bodies of Yaw and Large Pressure Gradient in High-Speed Flow," TN D-625, 1961, NASA.

[8] Hayes, W. D. and Probstein, R. F., *Hypersonic Flow Theory*, Academic Press, New York, 1959.

[9] Rosenhead, L., *Laminar Boundary Layers*, Clarendon Press, 1965.

[10] Moore, F. K., "Theory of Laminar Flows," *High Speed Aerodynamics and Jet Propulsion*, Vol. IV, Princeton Univ. Press, 1964.

[11] Clutter, D. W. and Smith, A. M. O., "Solutions of the General Boundary-Layer Equations for Compressible Laminar Flow, Including Equilibrium Dissociation," Paper 1657, Wash., D.C., 1963, Douglas Aircraft Co.

[12] Smith, A. M. O. and Clutter, D. W., "A General Method for Solving the Compressible Laminar Boundary-Layer Equations," Paper 1699, Liege, Belgium, 1963, Douglas Aircraft Co.

[13] Marvin, J. G. and Sinclair, R. A., "Convective Heating in Regions of Large Favorable Pressure Gradient," *AIAA Journal*, Vol. 5, No. 11, Nov. 1967, pp. 1940–1948.

[14] Lees, L., "Laminar Heat Transfer Over Blunt-Nose Bodies at Hypersonic Flight Speeds," *Jet Propulsion*, Vol. 26, 1956, pp. 259–269, 274.

[15] Polek, T. E., Holdaway, G. H., and Kemp, J. H., Jr., "Flow Field and Surface Pressures on a Blunt Half-Cone Entry Configuration at Mach Numbers of 7.4 and 10.4," TM X-1014, 1964, NASA.

[16] Winkler, E. M., "Stagnation Temperature Probes for Use at High Supersonic Speeds and Elevated Temperatures," Rept. 3834, 1954, U.S. Naval Ordnance Lab., White Oak, Md.

[17] Inouye, M., Rakich, J. V., and Lomax, H., "A Description of Numerical Methods and Computer Programs for Two-Dimensional and Axisymmetric Supersonic Flow Over Blunt Nosed and Flared Bodies," TN D-2970, 1965, NASA.

JANUARY 1970 AIAA JOURNAL VOL. 8, NO. 1

Distribution of a Trace Element in a Boundary Layer with Mass Transfer

NELSON H. KEMP* AND JAMES WALLACE†
Avco Everett Research Laboratory, Everett, Mass.

A theory is presented for the downstream distribution of a tracer injected into a boundary layer of a flat plate or cone with self-similar mass transfer. The tracer, which is injected over a finite length of the surface, is assumed to be chemically inert. Its behavior is controlled by a frozen diffusion equation. The assumption of constant density-viscosity product, and unit Schmidt number results in a linear partial differential equation for the seed mass fraction. This is solved analytically in series form by separation of variables, and numerically by a finite difference technique. It is shown that far downstream of the tracer injection region the analytical results reduce to a simple form; namely, the mass concentration profile is proportional to the local shear even in the presence of mass transfer. However, near the tracer injection region, even the first ten terms are insufficient to yield profiles comparable to those produced by the numerical integration scheme.

Nomenclature

C = trace species
D = diffusion coefficient
f = Blasius function with mass transfer
M = total mass rate of injection of trace species
N = eigenfunction with mass transfer
u,v = velocity components along and normal to the surface
x,y = Cartesian coordinates along and normal to the surface
z = transformed similarity variable
ξ,η = similarity variables
λ = eigenvalue
ϕ = mass fraction of tracer in ablating material
ρ = density
μ = coefficient of viscosity
$(\rho v)_w$ = mass transfer at solid surface

Subscripts

e = outer edge of boundary layer
h = trailing edge of injection region
i = leading edge of injection region
w = wall

Received May 12, 1969. This research was supported by the Advanced Research Projects Agency of the Department of Defense and Space and Missile Systems Organization, Air Force Systems Command, and was monitored by Space and Missile Systems Organization, Air Force Systems Command, under Contract F04701-68-C-0036.

* Principal Research Scientist; now Senior Consulting Scientist, Avco Systems Division, Wilmington, Mass. Associate Fellow AIAA.

† Senior Scientist. Member AIAA.

I. Introduction

THIS report investigates the problem of seeded boundary layers with mass transfer, i.e., boundary layers into which small amounts of foreign material are injected and used as tracers. Since the tracer is injected from a limited portion of a surface its concentration profile is different from the other species in the boundary layer. In this report we consider the simplest case of this problem, i.e., injection of a tracer into the boundary layer of a flat plate or cone and adopt the frequently employed approximation of constant $\rho\mu$ and unit Schmidt number in the boundary layer. The velocity profile in the ablating boundary layer then is uncoupled from the species equation and is approximated by the solution of the Blasius equation with mass transfer. The distribution of tracer in the boundary layer is described then by a linear nonsimilar diffusion equation whose coefficients depend upon the solution of the momentum equation. The problem thus formulated has been investigated previously in the case of zero blowing where it corresponds to diffusion with variable wall catalyticity, and to heat transfer to a wall with variable temperature.[1] The formulation of the problem with mass transfer is given in Sec. II.

The problem is investigated both numerically and analytically. The numerical solution is given in Sec. III,